Desalination and Water Treatment
www.deswater.com

doi:10.5004/dwt.2020.25168

182 (2020) 359–364
April

Photocatalytic degradation of organic dyes using nickel oxide incorporated titania nanocatalyst

Lalitha Gnanasekaran[a], R. Hemamalini[a,*], Saravanan Rajendran[b,*], Mu. Naushad[c], Jiaqian Qin[d], F. Gracia[e], Lorena Cornejo[b]

[a]*Department of Physics, Queen's College, Chennai-600 004, India, emails: hemaphy.qmc@gmail.com (R. Hemamalini), lalitha1887@gmail.com (L. Gnanasekaran)*
[b]*Faculty of Engineering, Department of Mechanical Engineering, University of Tarapacá, Avda, General Velasquez, 1775, Arica, Chile, emails: saravanan3.raj@gmail.com (S. Rajendran), lcornejoponce3@gmail.com (L. Cornejo)*
[c]*Department of Chemistry, College of Science, Building#5, King Saud University, Riyadh, Saudi Arabia, email: mnaushad@ksu.edu.sa*
[d]*Metallurgy and Materials Science Research Institute, Chulalongkorn University, Bangkok 10330, Thailand, email: jiaqianqin@gmail.com*
[e]*Department of Chemical Engineering, Biotechnology and Materials, University of Chile, Beauchef 851, 6th floor, Santiago, Chile, email: fgracia@ing.uchile.cl*

Received 31 December 2018; Accepted 11 November 2019

ABSTRACT

In this present work, two-step methods were executed to prepare TiO_2/NiO nanocomposite material. The selected area electron diffraction and X-ray diffraction pattern were interpreted and their fallouts demonstrate the occurrence of the tetragonal structure of TiO_2 beside the cubic structure of NiO. The NiO nanoparticles were randomly distributed on the surface of TiO_2 which was seen by transmission electron microscopy (TEM) and elemental mapping analyses. The high-resolution scanning electron microscope (HR-SEM) images of the prepared materials represent the spherical-shaped nanoparticles. The prepared TiO_2/NiO material shows high purity because it contains Ni, Ti and O elements without impurities which were represented by energy-dispersive X-ray spectroscopy. The estimated band gap of the prepared TiO_2@NiO nanocomposite is in the UV region. Under UV light condition, the nanocomposite effectively exploits the colorful dyes like methylene blue and methyl orange. In addition, their photocatalytic mechanism has been explained in detail.

Keywords: Photocatalyst; Degradation; UV light; Methyl orange; Nanocomposites

1. Introduction

The primary principle of the binary semiconductor system is controlled by oxidation and reduction potentials or energy levels of the two suitable systems. Hence, the favorable bandgap of two semiconductors is a prime factor to disturb the charge recombination process by the way of electron hopping mechanism. Furthermore, a suitable combination of two systems finds a way to produce more electrons and holes which powerfully demolish the organic pollutants under UV or visible light illuminations [1–4]. In recent years, various titania (TiO_2) based binary nano-semiconductor schemes like TiO_2/CuO, TiO_2/NiO, TiO_2/CeO_2, TiO_2/SnO_2, TiO_2/Fe_3O_4, TiO_2/ZnO showed superior photocatalysis [1–4]. Under UV light, Cheng et al. [5] defined that type II heterostructure (TiO_2/ZnO) material promotes a fine interface to boost the photocatalytic activity and effectively degraded the methylene blue solution. The coupling of TiO_2 with the CeO_2 system generated more electrons-holes which results in enhanced photocatalytic activity [6]. Also, the titania (TiO_2) based composite materials have exposed outstanding results in various fields such as solar cells hydrogen generation, biosensors, antibacterial activity and so on [1–9].

* Corresponding authors.

Still, the researchers are facing a real challenge to find the capable material for effective photocatalyst. Therefore, the target of existing work is to develop an effective catalyst for the photocatalytic reaction. Recently, nickel oxide (NiO) is presented with outstanding results for various applications in which it is being a p-type large bandgap (~3.6 eV) semiconducting and low-cost material. Moreover, when NiO incorporated with TiO_2 produced p-n junctions which extremely help to prevent the electrons-holes recombination resulting in enhanced photocatalytic activity [10]. For the aforementioned reasons, this work is focused on synthesis p-n semiconductor. In this scenario, the nanosized NiO/TiO_2 binary system was synthesized by two-step methods. Initially, the precipitation method was adopted to synthesize NiO. Additionally, the sol–gel method was employed to prepare the final TiO_2/NiO nanocomposite system. Several physical and chemical techniques were used (photoluminescence (PL), Brunauer–Emmett–Teller (BET) surface area and UV-Vis, X-ray diffraction (XRD), TEM and energy-dispersive X-ray spectroscopy (EDS))) to evaluate the properties of TiO_2, NiO, and TiO_2/NiO composite materials. The present work requires that the prepared catalyst has to be applied for the degradation of textile dyes under UV illumination and their consequences were discussed in detail.

2. Experimental

2.1. Preparation of TiO_2, NiO and TiO_2/NiO nanomaterials

Nickel nitrate, citric acid, isopropyl alcohol, titanium tetraisopropoxide, sodium hydroxide, methylene blue, and methyl orange were purchased from Sigma-Aldrich-Santiago, Chile. Further, the required aqueous solutions were prepared using double distilled water.

At first, the sol–gel method has been implemented to synthesize TiO_2 nanoparticles which were briefly discussed in our previous studies [7,8]. Further, NiO nanoparticles were synthesized by precipitation method. In this method, nickel nitrate (0.1 M) powder was dissolved in 100 ml of double-distilled water. Then, the pH of the dissolved nickel nitrate solution was increased by alkali solution (0.1 M of sodium hydroxide) under 600 rpm stirring conditions. As a result, precipitation occurred at the bottom of the beaker. Then the powder was washed and extracted from the solution by centrifugation. At last, the obtained greenish powder was dried and calcined at 550°C for 2 h.

For the TiO_2/NiO nanocomposite preparation; 5:0.2:1 of isopropanol, NiO (obtained from the precipitation method described above), and titanium tetraisopropoxide, were mixed and stirred for 2 h. Further, dropwise 0.1 M aqueous citrate was added into the above-mixed solution. Slowly the mixed solution was transformed to greenish-white gel which was dried and the collected greenish-white powder was calcined at 550°C for 2 h. In this manuscript, TiO_2, NiO and TiO_2/NiO were synthesized and symbolized as PT, PN, and TN respectively.

2.2. Photocatalytic experiment

In this present study, an 8W mercury vapor lamp was used for the UV source. The prepared materials were used as a catalyst for the degradation process. The explanation of photocatalytic experimental studies was described in our previous literature [7,8]. The concentration of dye and catalyst is 5×10^{-5} mol/L and 100 mg/L respectively. The photo irradiated dye solutions were kept in a 5 ml bottle at uniform time (every 10 min) intervals. After that, the solution was centrifuged and filtered for the extraction of catalyst from the irradiated solution. Furthermore, the absorbance behavior of the Methyl orange (MO) and Methylene Blue (MB) solutions was monitored by UV-Vis spectrometer.

2.3. Characterization details

The structure and purity of the synthesized catalysts were examined by an X-ray diffractometer (D5000 diffractometer, Siemens, USA) with $CuK_{\alpha 1}$ (λ = 1.5406 Å). The interface and size of the NiO and TiO_2 materials were investigated via TEM, FEI TITAN-Santiago, Chile G2 80-300 operated at 300 KeV. The bandgap and degradation of MO and MB were scrutinized by UV-Vis Spectrophotometry (Perkin Elmer Lambda 35). The emission property of the catalysts was explored via PL spectra which were recorded using a spectrophotometer (PerkinElmer Spectrofluorometer LS-55-USA). The specific surface area value of the catalyst was determined by Micromeritics ASAP 2020 (USA) at 77 K.

3. Result and discussion

The structural information of the synthesized catalysts was scrutinized by powder XRD measurement. Fig. 1a shows the XRD pattern of PT and their consistent JCPDS number is 21-1272. The indexed PT diffraction pattern describes the tetragonal structure and their corresponding lattice parameters; a = 3.810 Å and b = 9.410 Å. For PN material (Fig. 1b), the 2θ values were at 37.6°, 43.7° and 63.3° and their finely projected JCPDS number is 47-1049. The hkl planes of PN material are (111), (200) and (220) with a cubic-face centered structure and space group $Fm\bar{3}m$ (225); the determined lattice constant was $a = b = c$ = 4.180 Å.

The XRD pattern of binary composite oxide TN (shown in Fig. 1c) consists of TiO_2 diffraction peaks along with NiO peak (emphasized in the circle) at 43.7°. The addition of NiO material did not interrupt the anatase-tetragonal structure of TiO_2. But, the diffraction peaks are moved to a higher angle which is symbolized that the mismatch of ionic radii between both materials and formation of hybrid structure,

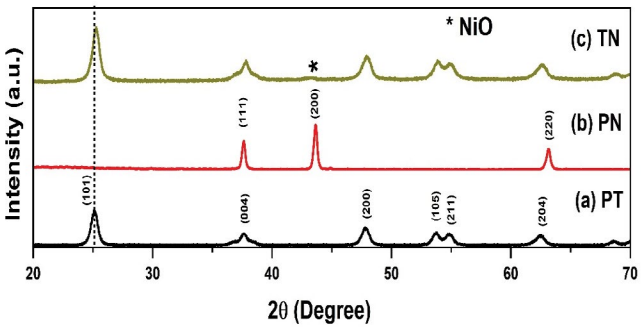

Fig. 1. X-ray diffraction pattern of (a) PT, (b) PN, and (c) TN.

that is, a tetragonal structure in addition to a cubic structure. The Scherrer formula was used to calculate the crystallite sizes of the catalysts [7] (which are represented in Table 1).

The XRD outcomes revealed that the synthesized TN material has dual structure and the particle is in nanosize. Compared with pure phases, the nanocomposite showed a small crystallite size. The outcome was further identified via TEM and BET analyses. The BET specific surface area values of the prepared PT, PN, and TN are described in Table 1 in which it was proved that the TN value is higher while compared with PT and PN. Because the NiO nanostructure prevents the growth of TiO_2 which led to the synergistic effect or interface between two different oxides ([1–4,9,10]. The HR-SEM images of the prepared PT, PN, and TN are shown in Fig. 2. All the prepared catalysts were spherical. Associated with PT and PN size, the TN material has exposed fine tiny particles. From the HR-SEM images, the particle size distribution curves mirrored the size of prepared materials and their respective values are depicted in Table 1. The TN material has expressed a small size that leads to promote higher surface area [11–13]. This higher surface area was confirmed by the BET technique (Table 1). Although associated with the pure system (PT and PN), the composite (TN) material has shown a smaller size due to the synergetic effect and interaction between NiO and TiO_2.

The TEM image of TN material suggests that a lot of small fine NiO spherical particles were mixed or spread on the TiO_2 nanoparticles (Fig. 3a). Reliable selected area electron diffraction (SAED) diffraction (Fig. 3b) pattern displays (101), (004) and (105) planes which express tetragonal TiO_2 (ICDD No: 21-1272) along with (111) and (200) planes for cubic NiO (ICDD No: 47-1049) structure. Further, the elemental mapping results (Fig. 3c) indicate that NiO and TiO_2 materials were mixed consistently with the highly developed interfaces [14,15]. The energy-dispersive X-ray spectroscopy (EDXS) result in Fig. 3c confirmed the presence of Ni, Ti and O elements in the TN system. The inserted images in Fig. 3c represents the elemental mapping of TN material that exposed the regular distribution of Ti, Ni and O elements.

Table 1
Particle size, band gap, surface area and degradation results of the prepared materials

Samples	Crystallite size (nm)		HR-SEM particle size (nm)		BET-surface area (m^2/g)	Optical band gap	Removal of MO (%)	Removal of MB (%)
	TiO_2	NiO	TiO_2	NiO		eV	60 min	60 min
PT	28.4	–	25	–	65.2	3.20	58	62.4
PN	–	33	–	30	25.2	3.60	35.2	39.4
TN	17.5	11.8	14	10	100.3	3.44	92.4	98.3

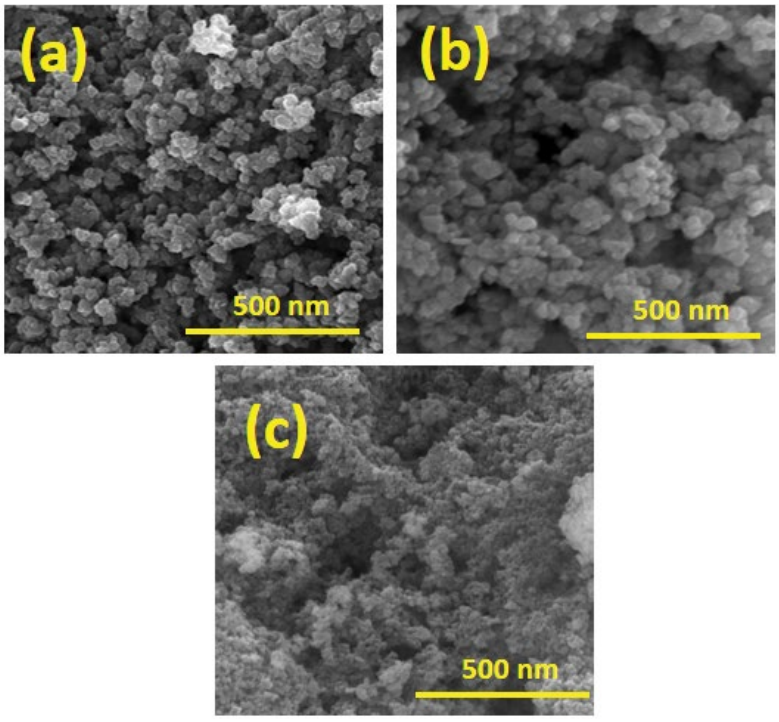

Fig. 2. HR-SEM images of (a) PT, (b) PN, and (c) TN nanomaterials.

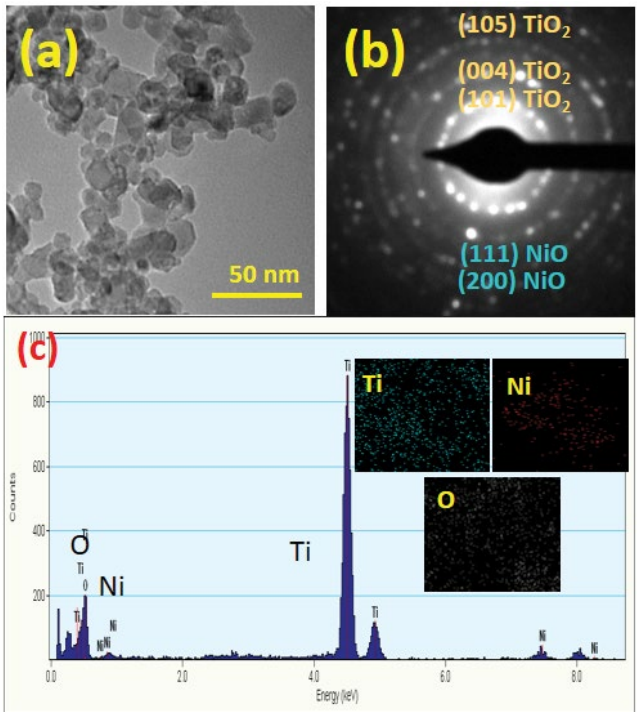

Fig. 3. TN nanomaterials (a) TEM, (b) SAED, and (c) EDXS results.

The UV-Vis absorption spectra of the synthesized TN material show the dual dissimilar absorption edges. In Fig. 4, the core edge of the TN seems to be present at 385 nm (which refers to TiO_2 material) and the minor edge (decorated in the circle) at 345 nm is due to NiO content in the TN material [7,8,16–18]. In this prepared nanocomposite, band edges appeared in the UV region. However, compared with the PT system, the absorption edge has extended due to the transition of electrons in-between two different energy levels (NiO and TiO_2). Thus, the excitation of the valence band (VB) electrons of PT and TN materials primarily trust the source of UV light [14,19]. Also, the dual-energy gap system has the capability to postpone the electrons-holes recombinations [14,19].

The result of PL spectroscopy helps to estimate the charge recombination process and migration of electrons behavior using a 330 nm excitation wavelength. The PL (Fig. 5) spectra of PT showed the emission band at 425 nm which indicates the surface recombination of TiO_2 [16,20]. The band at 470, 490 and 540 nm show the surface oxygen vacancies [16,20]. The emission intensity has greatly diminished after the incorporation of NiO into the TiO_2 structure. The substantially reduced intensity suggested that the recombination process has been delayed by an intermediate band. The hindering is preferred for the superior photocatalytic activity [5,16,18,20].

3.1. Photocatalytic degradation of MO and MB

The target of the present study is to prepare an effective catalyst for the photocatalytic reaction. In this connection, the prepared catalyst has been effectively used for the degradation of MO and MB dyes because these organic dyes (anionic and cationic) are mostly used for textile industries. The TN nanocomposites have displayed (Table 1) a higher degradation rate of MO and MB dyes. The degradation fallouts were analogous with prior reports and the consequence was displayed in (Table 2). On associating with described degradation values [10,21–26], this study shows better degradation within short duration due to the size and hindering of electron-hole recombinations which were achieved by the formation of p-n junction [3,10].

The bandgap of all the prepared materials exist in the UV region. However, the TN nanocomposite consists of NiO and TiO_2 materials with two different band edges at 345 and 385 nm respectively (from UV-Vis absorbance result). In this study, UV light (365 nm) is used which is near to NiO and TiO_2 wavelengths and their schematic illustration (Fig. 6) explained the perfect electrons and holes movement.

The excitation of the VB electrons of TiO_2 has transferred to the adjoining VB of NiO. Concurrently, the excitation

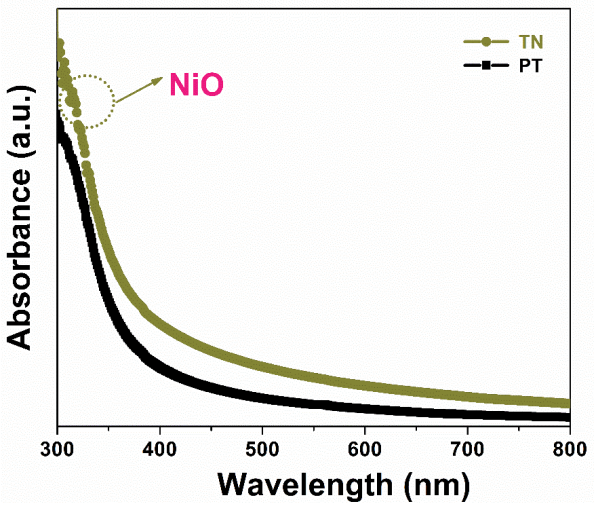

Fig. 4. UV-Vis absorbance results of PT and TN nanomaterials.

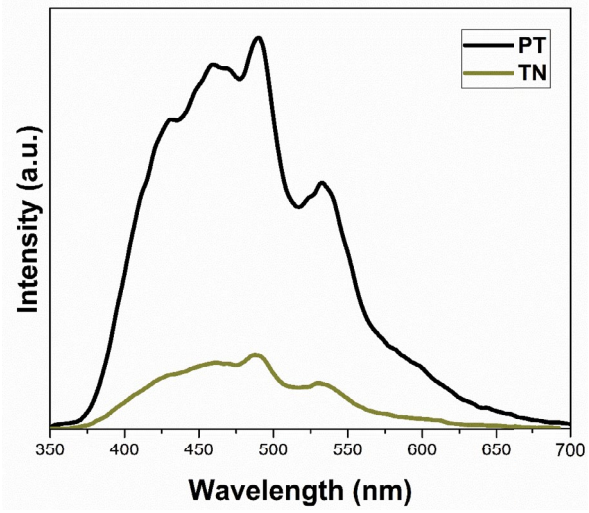

Fig. 5. PL results of PT and TN nanomaterials.

Table 2
Comparison of degradation results with previous reports

Material	Method	Shape	Degradation dyes	Efficiency	References
NiO/TiO_2	Incipient wetness impregnation	–	MB	85% for 5 h (UV light)	[10]
NiO/TiO_2	Incipient wet impregnation method	Nanotubes	MB	83% for 450 min (UV light)	[21]
NiO/TiO_2	Templates	Mesoporous shells	MB	90% for 100 min (visible light)	[22]
NiO/TiO_2	Thin Film	Nano spherical	MB	45% for 120 (UV light)	[23]
NiO/TiO_2	Modified ammonia-evaporation-induced synthetic method	Nano spherical	MB	50% for 30 min (UV light)	[24]
NiO addition in TiO_2	Sol–gel	–	MB	92.85% for 360 min (visible light)	[25]
NiO/TiO_2	Chemical-solution-deposition-decomposition process	Nano cluster	MO	98% for 180 min (visible light)	[26]
TiO_2/NiO	Precipitation-sol gel	Nano spherical	MO and MB	92.4% for 60 min (MO) 98.3% for 60 min (MB)	In this study

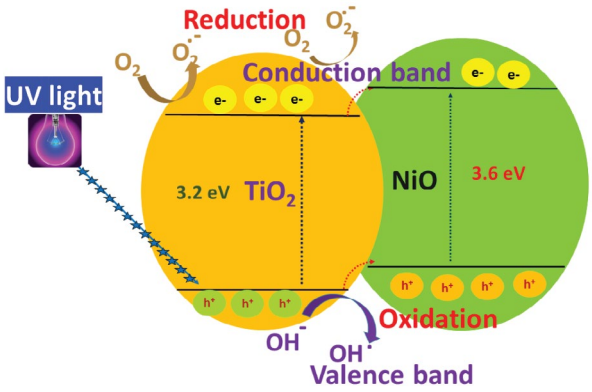

Fig. 6. Pictorial representation of photocatalytic activity of TN material.

has happened from VB of NiO, because the NiO wavelength (345 nm) is near to the irradiation light (365 nm). Consequently, the excited electrons were interchanged to Conduction Band (CB) of TiO_2 and vice versa CB of NiO. In this process, the stimulated electrons and holes vigorously started the oxidation and reduction, which lead to producing more hydrogen peroxides which can easily destroy the structure of MO and MB dyes [27–30]. Additionally, the survival of dual-energy states supported the superior photocatalytic activity via delaying the electrons-holes recombination. (proved by PL spectrometer). Furthermore, the synergistic effect between TiO_2 and NiO tends to reduce the size of the material and boosts the surface properties which leads to an increase the photocatalytic activity [21–37].

4. Conclusion

The TiO_2/NiO nanocomposite material was prepared by innovative two-step methods. The characteristics of nanocomposite TiO_2/NiO revealed that the prepared catalysts exhibited a cubic structure of NiO nanoparticles randomly incorporated on the surface of TiO_2. The absorption edges marked that the synthesized TiO_2/NiO catalyst is very strong in the UV region and ensured the dual-energy states. The TEM and HR-SEM images showed spherical shaped nanoparticles. When compared with TiO_2 and NiO materials, the TiO_2/NiO catalyst displayed a higher degradation rate under UV light illumination and vigorously damaged the structure of colorful contaminants. The superior photocatalytic outcomes were achieved via the formation of the p-n junction and strong interfaces between the two systems which are the prime factors in retarding the electron-hole recombination.

Acknowledgments

We acknowledge Dr. K. Ravichandran, Department of Nuclear Physics, University of Madras, India for the lab facilities and his valuable contribution to the discussion. The authors (S.R., F.G.) acknowledge the support of CONICYT through the project CONICYT/FONDAP/15110019. The author (S.R) acknowledge the FONDECYT Government of Chile (Project No.: 11170414), for the support to carry out this project and One of the authors (Mu. Naushad) is grateful to the Researchers Supporting Project number (RSP-2019/8), King Saud University, Riyadh, Saudi Arabia for the support.

References

[1] N. Mufti, U. Munfarriha, A. Fuad, M. Diantoro, Synthesis and photocatalytic properties of Fe_3O_4@TiO_2 core-shell for degradation of Rhodamine B, AIP Conf. Proc., 1712 (2016) 50009.
[2] A.L. Luna, M.A. Valenzuela, C. Colbeau-Justin, P. Vázquez, J.L. Rodriguez, J.R. Avendaño, S. Alfaro, S. Tirado, A. Garduño, J.M. De La Rosa, Photocatalytic degradation of gallic acid over CuO–TiO_2 composites under UV/Vis LEDs irradiation, Appl. Catal., A, 521 (2016) 140–148.
[3] M. Wang, Y. Hu, J. Han, R. Guo, H. Xiong, Y. Yin, TiO_2/NiO hybrid shells. p–n junction photocatalysts with enhanced activity under visible light, J. Mater. Chem. A, 3 (2015) 20727–20735.
[4] H. Tada, A. Hattori, Y. Tokihisa, K. Imai, N. Tohge, S. Ito, A patterned-TiO_2/SnO_2 bilayer type photocatalyst, J. Phys. Chem. B, 104 (2000) 4585–4587.

[5] C. Cheng, A. Amini, C. Zhu, Z. Xu, H. Song, N. Wang, Enhanced photocatalytic performance of TiO_2-ZnO hybrid nanostructures, Sci. Rep., 4 (2014) 4181.
[6] H. Eskandarloo, A. Badiei, M.A. Behnajady, TiO_2/CeO_2 hybrid photocatalyst with enhanced photocatalytic activity. Optimization of synthesis variables, Ind. Eng. Chem. Res., 53 (2014) 7847–7855.
[7] L. Gnanasekaran, R. Hemamalini, K. Ravichandran, Synthesis and characterization of TiO_2 quantum dots for photocatalytic application, J. Saudi Chem. Soc., 19 (2015) 589–594.
[8] L. Gnanasekaran, R. Hemamalini, R. Saravanan, K. Ravichandran, F. Gracia, S. Agarwal, V.K. Gupta, Synthesis and characterization of metal oxides (CeO_2, CuO, NiO, Mn_3O_4, SnO_2 and ZnO) nanoparticles as photo catalysts for degradation of textile dyes, J. Photochem. Photobiol. B, 173 (2017) 43–49.
[9] P. Dhiman, M. Naushad, K.M. Batoo, A. Kumar, G. Sharma, A.A. Ghfar, G. Kumar, M. Singh, Nano $Fe_xZn_{1-x}O$ as a tuneable and efficient photocatalyst for solar powered degradation of bisphenol A from aqueous environment, J. Cleaner Prod., 165 (2017) 1542–1556.
[10] C.-J. Chen, C.-H. Liao, K.-C. Hsu, Y.-T. Wu, J.C.S. Wu, P–N junction mechanism on improved NiO/TiO_2 photocatalyst, Catal. Commun., 12 (2011) 1307–1310.
[11] V.K. Gupta, R. Saravanan, S. Agarwal, F. Gracia, M. Mansoob Khan, J. Qin, R.V. Mangalaraja, Degradation of azo dyes under different wavelengths of UV light with chitosan-SnO_2 nanocomposites, J. Mol. Liq., 232 (2017) 423–430.
[12] R. Saravanan, V.K. Gupta, V. Narayanan, A. Stephen, Comparative study on photocatalytic activity of ZnO prepared by different methods, J. Mol. Liq., 181 (2013) 133–141.
[13] J. Schneider, M. Matsuoka, M. Takeuchi, J. Zhang, Y. Horiuchi, M. Anpo, D.W. Bahnemann, Understanding TiO_2 photocatalysis: mechanisms and materials, Chem. Rev., 114 (2014) 9919–9986.
[14] A.C. Pradhan, T. Uyar, Morphological control of mesoporosity and nanoparticles within Co_3O_4–CuO electrospun nanofibers. quantum confinement and visible light photocatalysis performance, ACS Appl. Mater. Interf., 9 (2017) 35757–35774.
[15] L. Qi, B. Cheng, J. Yu, W. Ho, A review on TiO_2-based Z-scheme photocatalysts, Chin. J. Catal., 38 (2017) 1936–1955.
[16] C. Mercado, Z. Seeley, A. Bandyopadhyay, S. Bose, J.L. McHale, Photoluminescence of dense nanocrystalline titanium dioxide thin films. Effect of doping and thickness and relation to gas sensing, ACS Appl. Mater. Interf., 3 (2011) 2281–2288.
[17] R. Saravanan, V.K. Gupta, V. Narayanan, A. Stephen, Visible light degradation of textile effluent using novel catalyst ZnO/γ-Mn_2O_3, J. Taiwan Inst. Chem. Eng., 45 (2014) 1910–1917.
[18] R. Saravanan, N. Karthikeyan, V.K. Gupta, E. Thirumal, P. Thangadurai, V. Narayanan, A. Stephen, ZnO/Ag nanocomposite. An efficient catalyst for degradation studies of textile effluents under visible light, Mater. Sci. Eng. C, 33 (2013) 2235–2244.
[19] D. Zhao, X. Wu, Nanoparticles assembled SnO_2 nanosheet photocatalysts for wastewater purification, Mater. Lett., 210 (2018) 354–357.
[20] P.C. Ricci, C.M. Carbonaro, A. Geddo Lehmann, F. Congiu, B. Puxeddu, G. Cappelletti, F. Spadavecchia, Structure and photoluminescence of TiO_2 nanocrystals doped and co-doped with N and rare earths (Y^{3+}, Pr^{3+}), J. Alloys Comp., 561 (2013) 109–113.
[21] L.M. Sim, K.W. Ng, S. Ibrahim, P. Saravanan, Preparation of improved p-n junction NiO/TiO_2 nanotubes for solar-energy-driven light photocatalysis, Int. J. Photoenergy, 659013 (2013) 1–10.
[22] M. Wang, J. Han, Y. Hu, R. Guo, Y. Yin, Carbon-Incorporated NiO/TiO_2 Mesoporous shells with p–n heterojunctions for efficient visible light photocatalysis, ACS Appl. Mater. Interf., 8 (2016) 29511–29521.
[23] J.Z. Chen, T.H. Chen, L.W. Lai, P.Y. Li, H.W. Liu, Y.Y. Hong, D.H. Liu, Preparation and characterization of surface photocatalytic activity with NiO/TiO_2 nanocomposite structure, Materials, 8 (2015) 4273–4286.
[24] K. Chockalingam, A. Ganapathy, G. Paramasivan, M. Govindasamy, NiO/TiO_2 nanoparticles for photocatalytic disinfection of bacteria under visible light, J. Am. Ceram. Soc., 94 (2011) 2499–2505.
[25] S. Wahyuningsih, A.H. Ramelan, P.D. Purwanti, H. Munawaroh, S. Ichsan, Y.R. Kristiawan, The influence of NiO addition in TiO_2 structure and its photoactivity, IOP Conf. Ser.: Mater. Sci. Eng., 333 (2018) 012032.
[26] L. Chu, M. Li, P. Cui, Y. Jiang, Z. Wan, S. Dou, The study of NiO/TiO_2 photocatalytic activity for degradation of methylene orange, Energy Environ. Focus, 3 (2014) 371–374.
[27] A.Y. Shan, T.I.M. Ghazi, S.A. Rashid, Immobilisation of titanium dioxide onto supporting materials in heterogeneous photocatalysis: a review, Appl. Catal., A, 389 (2010) 1–8.
[28] G. Sharma, A. Kumar, Mu. Naushad, A. Kumar, A.H. Al-Muhtaseb, P. Dhiman, A.A. Ghfar, F.J. Stadler, M.R. Khan, Photoremediation of toxic dye from aqueous environment using monometallic and bimetallic quantum dots based nanocomposites, J. Cleaner Prod., 172 (2018) 2919–2930.
[29] M. Shekofteh-Gohari, A. Habibi-Yangjeh, Combination of $CoWO_4$ and Ag_3VO_4 with Fe_3O_4/ZnO nanocomposites. Magnetic photocatalysts with enhanced activity through p-n-n heterojunctions under visible light, Solid State Sci., 74 (2017) 24–36.
[30] F. Shi, Y. Li, Q. Zhang, H. Wang, Synthesis of $Fe_3O_4/C/TiO_2$ Magnetic photocatalyst via vapor phase hydrolysis, Int. J. Photoenergy, 365401 (2012) 1–8.
[31] M. Naushad, Surfactant assisted nano-composite cation exchanger: development, characterization and applications for the removal of toxic Pb^{2+} from aqueous medium, Chem. Eng. J., 235 (2014) 100–108.
[32] J. Mohanraj, D. Durgalakshmi, S. Balakumar, P. Aruna, S. Ganesan, S. Rajendran, M. Naushad, Low cost and quick time absorption of organic dye pollutants under ambient condition using partially exfoliated graphite, J. Water Process. Eng., (2019) 101078. https://doi.org/https://doi.org/10.1016/j.jwpe.2019.101078.
[33] E. Daneshvar, A. Vazirzadeh, A. Niazi, M. Kousha, M. Naushad, A. Bhatnagar, Desorption of Methylene blue dye from brown macroalga: effects of operating parameters, isotherm study and kinetic modeling, J. Cleaner Prod., 152 (2017) 443–453.
[34] Mu. Naushad, A.A. Alqadami, Z.A. AlOthman, I.H. Alsohaimi, M.S. Algamdi, A.M. Aldawsari, Adsorption kinetics, isotherm and reusability studies for the removal of cationic dye from aqueous medium using arginine modified activated carbon, J. Mol. Liq., 293 (2019) 111442.
[35] Z.A. AlOthman, R. Ali, M. Naushad, Hexavalent chromium removal from aqueous medium by activated carbon prepared from peanut shell: adsorption kinetics, equilibrium and thermodynamic studies, Chem. Eng. J., 184 (2012) 238–247.
[36] I. Mironyuk, T. Tatarchuk, M. Naushad, H. Vasylyeva, I. Mykytyn, Highly efficient adsorption of strontium ions by carbonated mesoporous TiO_2, J. Mol. Liq., 285 (2019) 742–753.
[37] M. Naushad, G. Sharma, Z.A. Alothman, Photodegradation of toxic dye using Gum Arabic-crosslinked-poly(acrylamide)/$Ni(OH)_2$/FeOOH nanocomposites hydrogel, J. Cleaner Prod., 241 (2019) 118263.